*Annals of Glaciology* 33 2001


# The Antarctic Circumpolar Wave in a global, high-resolution, coupled ice–ocean model

Yuxia Zhang, Albert J. Semtner
*Department of Oceanography, Naval Postgraduate School, Monterey, CA 93943, U.S.A.*

ABSTRACT. The Antarctic Circumpolar Wave (ACW) is identified by White and Peterson (1996) as anomalies in sea-level pressure, meridional wind stress (MWS), sea-surface temperature (SST) and sea-ice extent (SIE) propagating eastward over the Southern Ocean. In this study, the ACW is examined using a global coupled ice–ocean model with an average horizontal grid size of 1/4°. The model is forced with 1979–93 daily average atmospheric data from the European Centre for Medium-range Weather Forecasts (ECMWF) re-analysis (ERA). The sea-ice model includes both dynamics and thermodynamics, and the ocean model is a primitive-equation, free-surface, *z*-coordinate model. Both standing and propagating oscillations are present in ERA surface net heat-flux (NHF) and MWS anomalies. The ocean and ice respond to such atmospheric forcing with similar standing and propagating oscillations. For the propagating mode, SIE, SST and sea-surface salinity anomalies propagate eastward with a period of about 4–5 years and take about 8–9 years to encircle the Antarctic continent. Thus, the simulated ACW is a wavenumber-2 phenomenon which agrees with the ACW identified by White and Peterson (1996). The correctly simulated strength of the Antarctic Circumpolar Current, which governs the phase speed of oceanic anomalies, in our high-resolution model is essential for obtaining the observed wavenumber-2 ACW mode in the ocean. The ACW signature is also present in ocean temperature and salinity anomalies down to about 1000 m depth with similar eastward-propagating speed. The anomalies in the interior ocean are more coherent and intense over the Pacific and Atlantic sectors than over the Indian sector. Northward (southward) MWS anomalies, northward (southward) SIE anomalies, cold (warm) SST anomalies and saltier (fresher) than normal salinity anomalies are in phase, while less (more) than normal NHF is 90° out of phase with them, indicating the ACW in sea ice and ocean is a response to that in the atmosphere.

## 1. INTRODUCTION

The Antarctic Circumpolar Wave (ACW) is identified by White and Peterson (1996) as anomalies in sea-level pressure (SLP), meridional wind stress (MWS), sea-surface temperature (SST) and sea-ice extent (SIE) over the Southern Ocean, propagating eastward with a period of 4–5 years and taking 8–10 years to encircle the globe. Thus, it is a wavenumber-2 phenomenon. At about the same time, Jacobs and Mitchell (1996) found a similar ACW mode in anomalous sea-surface height from TOPEX/POSEIDON altimeter observations. The datasets used by White and Peterson (1996) consist of in situ and satellite measurements for SST and SIE, and 1985–94 European Centre for Medium-range Weather Forecasts (ECMWF) operational analyses for SLP and MWS. Utilizing 1979–94 ECMWF re-analysis (ERA) (a longer dataset as compared to the period covered by White and Peterson (1996)), Bonekamp and others (1999) identified both propagating and standing oscillations in SLP and MWS anomalies. For the period 1985–94, coinciding with the period studied by White and Peterson (1996), eastward propagation is present in more or less the same way as in the operational analysis used by White and Peterson (1996). However, during the earlier period 1979–84, the eastward propagation is absent, and the standing oscillations exist instead.

Unlike the wavenumber-2 ACW mode described by White and Peterson (1996), coupled climate-model studies by Christoph and others (1998) and Cai and others (1999) found a dominant wavenumber-3 pattern in atmospheric, oceanic and sea-ice variables. Although White and Peterson (1996) reported the phase-locking of observed ACW components (i.e. all anomalies propagate eastward at the same rate), the atmospheric anomalies in the studies of Christoph and others (1998) and Cai and others (1999) showed little or no eastward propagation, while the oceanic anomalies propagated eastward. The period of their oceanic ACW mode is 4–5 years, but it takes about 12–16 years for an anomaly to encircle the globe.

Several studies have tried to understand the dynamics of the ACW. Qiu and Jin (1997) and Peterson and White (1998) concluded that the ACW is a mode of the coupled atmosphere–ocean sea-ice system and that atmosphere–ocean interaction plays a dominant role in maintaining the ACW from dissipation as it travels around the globe. In the simulations of Qiu and Jin (1997) with a simple coupled atmosphere–ocean model, the atmosphere reacts to a warm SST anomaly with a high (low) SLP anomaly to the east (west) of it (see Qiu and Jin, 1997, plate 2). The corresponding wind-stress anomalies deepen (shallow) the ocean mixed layer by Ekman pumping, and the warm (cold) SST anomaly is strengthened by a warm (cold) geostrophic flow from the north (south). The whole anomaly system is advected with the Antarctic Circumpolar Current (ACC), and the SLP anomaly is phase-locked to the SST anomaly. Peterson and White (1998)



https://doi.org/10.3189/172756401781818644 Published online by Cambridge University Press

suggested that the ACW has a major source in the western subtropical South Pacific, where interannual anomalies in SST develop in response to the El Niño–Southern Oscillation (ENSO) near the Equator (see Peterson and White, 1998, fig. 1). Subsequently, these ENSO-scale SST anomalies propagate southward into the Southern Ocean in tandem with SLP anomalies. The system then migrates east around the globe through a combination of oceanic advection with the ACC and ocean–atmosphere coupling. In contrast to Peterson and White (1998), Christoph and others (1998) and Cai and others (1999) found that ENSO is not a significant source for the ACW. They argued that the ACW has its origins in the southern mid- to high latitudes.

Modeling studies cast doubt on the coupled atmosphere–ocean explanation of the ACW. The breakdown of phase-locking in atmospheric and oceanic components of the ACW in the coupled model studies of Christoph and others (1998) and Cai and others (1999) suggests that the feedback of SST anomalies on the atmospheric circulation is weak. Christoph and others (1998) concluded that the ACW represents the net result of propagating oceanic anomalies interacting with a spatially fixed resonant atmospheric background pattern such that the oceanic anomalies are selectively amplified or dissipated. Weisse and others (1999) used an ocean-only model driven by stochastic atmospheric forcing with a spatially fixed zonal wavenumber-3 pattern, and showed that the irregular atmospheric fluctuations in time are sufficient to excite propagating signals in the ocean surface layer, generating similar ACW patterns described by Christoph and others (1998). The large-scale spatial coherence of the atmospheric forcing and the average zonal velocity of the ACC determine the time-scale of the oceanic variability.

In this study, we examine the ACW using a global coupled ocean–ice model forced with the ERA data. Section 2 contains a brief description of the sea-ice and ocean models and the atmospheric forcing data. Section 3 presents the propagation characteristics of the ACW. Section 4 discusses the temporal phase relation among variables in atmosphere, ocean and sea ice. Conclusions are given in section 5.

## 2. MODEL DESCRIPTION

The global coupled ocean–ice model consists of two pieces: (1) an almost-global, primitive-equation, $z$-coordinate ocean model (Semtner and Chervin, 1992) with added free-surface (Killworth and others, 1991) and Antarctic sea ice; and (2) an Arctic ice–ocean model. The almost-global ocean model utilizes a Mercator grid with an average horizontal grid size of 1/4° (~20 km at 60° S or 60° N) and 20 vertical levels. The model bathymetry is obtained without applying any smoothing, which provides higher accuracy in mapping the true geometry onto the model domain. Due to numerical singularity at the Poles, the domain of the almost-global ocean model extends only from 75° S to 65° N, thus omitting the Arctic Ocean. The Antarctic sea-ice model employs a polar stereographic projection with a horizontal grid size of 18 km. It uses an elastic–viscous–plastic ice rheology (Hunke and Dukowicz, 1997; Hunke and Zhang, 1999) and the zero-layer approximation for heat conduction through ice (Semtner, 1976). The surface heat budget follows that of Parkinson and Washington (1979).

To complete the global model domain, the almost-global ocean model is adapted to the Arctic Ocean (Parsons, 1995; Maslowski, 1997) by transforming the Mercator grid into a rotated coordinate system, in which the model Equator passes through the geographic North Pole. It has a 1/6° (~18 km) horizontal grid size and 30 vertical levels. The model domain includes the Arctic Ocean, Barents and Kara Seas, Nordic Seas, Baffin and Hudson Bays, Canadian Archipelago, and subpolar North Atlantic Ocean (for more information on the model, see Zhang and others (1999)). The Arctic sea-ice model uses the same grid as the Arctic ocean model and has the same dynamics and thermodynamics as the Antarctic sea-ice model described earlier. The almost-global model is joined to the Arctic model by means of interpolating between the different model grids both horizontally and vertically, and exchanging lateral boundary information in the subpolar North Atlantic.

Following initialization with Levitus (1982) climatological temperature and salinity and uniform 2 m sea ice, the almost-global and the Arctic models were spun up separately for several decades. The 3-daily averaged ECMWF operational analysis was then used to force the two models for a decade. Finally, the two pieces of the ocean–ice model were run interactively for 15 years with daily-averaged ERA (1979–93) data (surface net heat flux, 10 m winds, precipitation and evaporation) as atmospheric forcing. The last 15 year model output is analyzed and presented here.

## 3. EASTWARD PROPAGATION

In this section, time–longitude diagrams of the monthly anomalies of net heat flux (NHF) at the surface of sea ice or open ocean, MWS at 10 m, SIE, and ocean temperature and salinity are shown (Fig. 1) to illustrate the eastward propagation characteristic of the ACW. As in White and Peterson (1996), the monthly anomalies in each variable at each grid-point are determined relative to the 15 year monthly mean values, thus removing the mean seasonal cycles. To further suppress the high- and low-frequency signals, the monthly anomalies are then filtered with a bandpass filter having a 3–7 year admittance window. All monthly anomalies are along 56° S except the SIE, which is for 5° longitude increments. No space filtering is employed. The sign convention used here is that positive values denote northward SIE anomalies, warm-ocean temperature anomalies, saltier than normal salinity, northward MWS anomalies and more than normal downward NHF.

We first examine the time–longitude diagrams of monthly anomalies of NHF and MWS from ERA (Fig. 1), which are used to drive the ocean–ice model. The NHF is the sum of net sensible- and latent-heat fluxes and net short- and long-wave radiations at the surfaces of sea ice or open ocean. The MWS is computed using the bulk aerodynamic formula with ERA 10 m winds and stability-dependent drag coefficient (Large and Pond, 1982). Consistent with the results from Bonekamp and others (1999), eastward propagations of NHF and MWS anomalies are present from about 1983. Prior to 1983, standing oscillations exist in both NHF and MWS anomalies. For the propagating mode, it takes about 8–9 years for an individual phase to travel around the globe, and variability at a particular location occurs on a time-scale of 4–5 years. Thus, the eastward-propagating NHF and MWS anomalies have a spatial length scale characterized by wavenumber 2, consistent with the findings by White and Peterson (1996). For the standing oscillation, a higher wave-


https://doi.org/10.3189/172756401781818644 Published online by Cambridge University Press

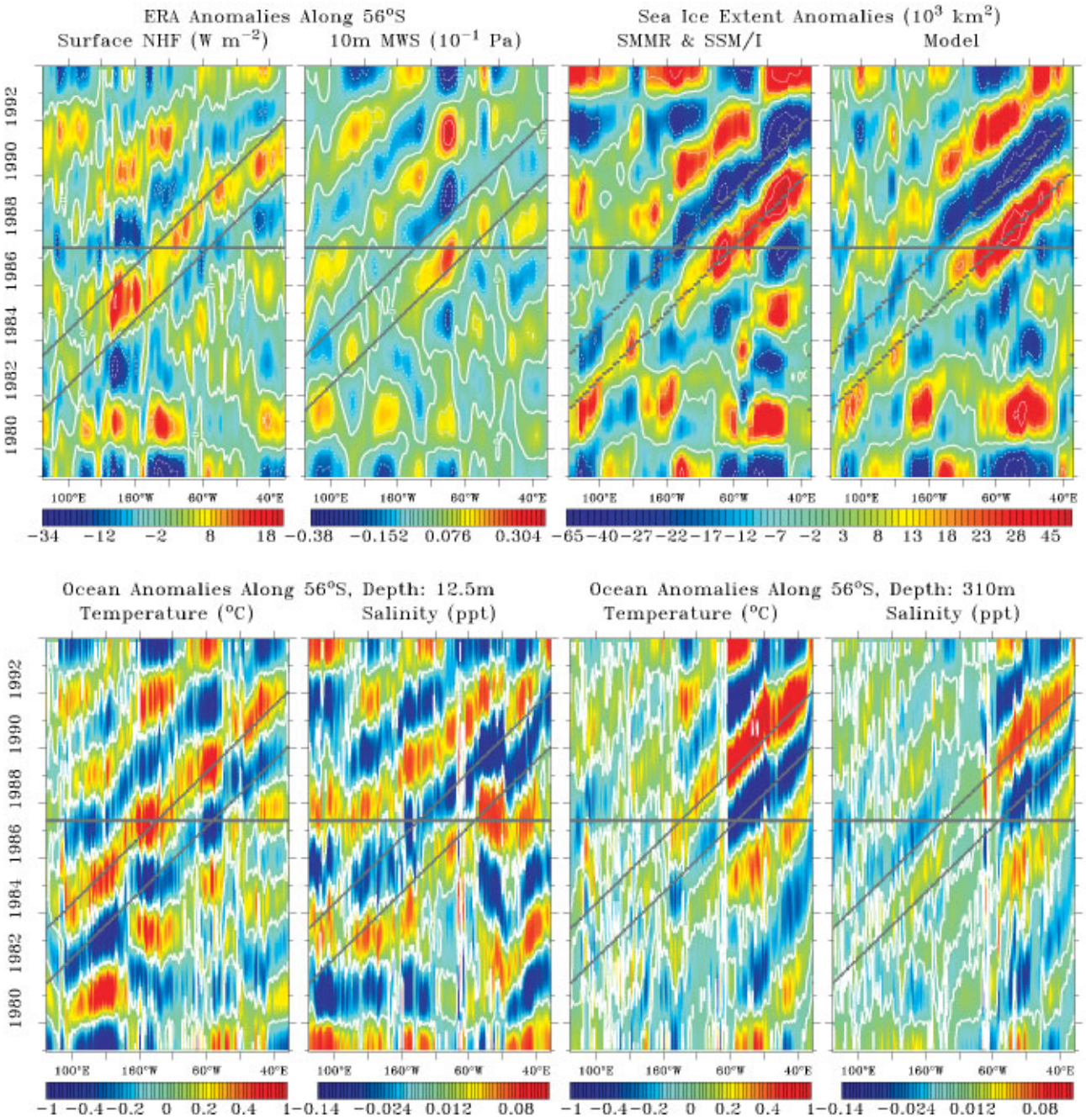


*Fig. 1. Time–longitude diagrams of the filtered monthly anomalies of surface net heat flux (NHF) and 10 m meridional wind stress (MWS) from ERA; sea-ice extent (SIE) from SMMR and SSM/I and the model; ocean temperatures and salinities at 12.5 m (mid-depth of the first level) and 310 m (mid-depth of the eighth level) from the model. The contour intervals are 10 W m$^{-2}$ for NHF, 0.01 Pa for MWS and 2000 km$^2$ for SIE. Only the zero contour lines are shown in the lower panels. The gray lines in all panels are synchronous in time and space.*

number (3–4) is present, resembling the atmospheric variability described by Christoph and others (1998).

Both the simulated and observed time–longitude diagrams of SIE anomalies are displayed in Figure 1. The observed SIE is obtained from the sea-ice concentration derived from the Scanning Multichannel Microwave Radiometer (SMMR) and Special Sensor Microwave/Imager (SSM/I) brightness temperatures using the NASA Team algorithm (Gloersen and others, 1992; Comiso and others, 1997). Similar to NHF and MWS anomalies, both standing and eastward-propagating oscillations are present in the SIE anomaly. The fact that the standing oscillation is also present in the satellite passive-microwave observations indicates that the sudden switching-on of the ERA forcing (see section 2) has little impact on the modeled SIE oscillation in the beginning of the time series. The propagating mode of the SIE anomaly has the same oscillation period and phase speed as the NHF and MWS anomalies, suggesting the presence of eastward propagation in the SIE anomaly is a response to that in the atmosphere. Notice that the simulated propagating and standing anomalies of the SIE are in very good agreement with the observed.

Like the SIE anomaly, the anomalies of the first-level (mid-depth: 12.5 m) ocean temperature and salinity (hereafter referred to as SST and SSS, respectively) also have a pronounced eastward propagation during the period 1983–93 (Fig. 1). There are indications of standing oscillation from 1979 to 1982, but the signal is not as clear as for the SIE.



https://doi.org/10.3189/172756401781818644 Published online by Cambridge University Press

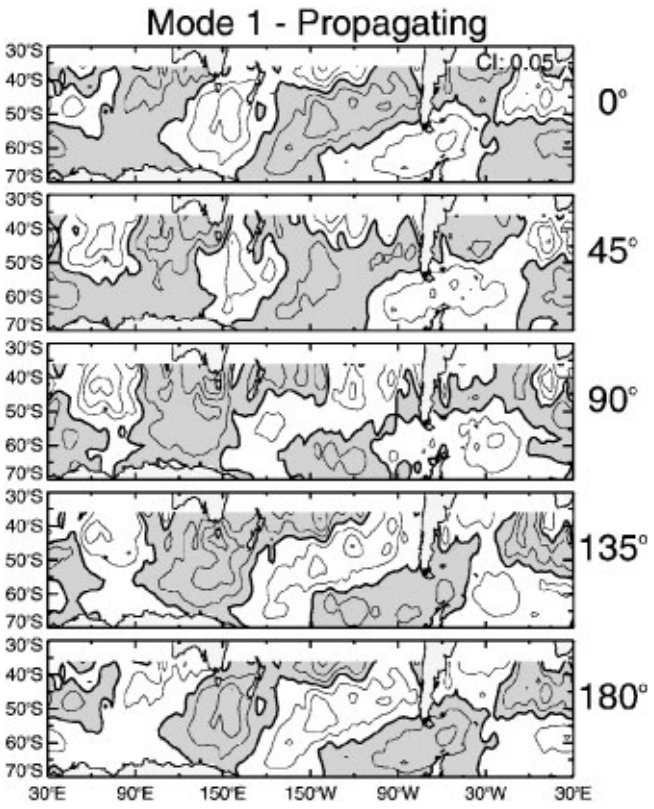


*Fig. 2. The 0°, 45°, 90°, 135° and 180° phases of the first mode (explains 59% of the total variance) of the propagating wave of CEOF analysis on the first-level (mid-depth: 12.5 m) ocean temperature. Positive (or warm) anomalies are shaded, and contour intervals are 0.05°C.*

Their phase speeds and oscillation periods are the same as those of SIE, NHF and MWS. The predominant wavenumber-2 pattern and the dominant time-scale of 4–5 years in the SST anomaly is illustrated further by its first complex empirical orthogonal function (CEOF) pattern (Fig. 2) and the corresponding temporal normalized amplitude (Fig. 3). The CEOF analysis (Preisendorfer, 1988) was conducted at our request by J. L. Annis of the Scripps Institution of Oceanography on the SST anomaly, filtered with a bandpass filter having a 3–6 year admittance window. A wave partitioning is then performed to separate the dominant modes of CEOF into standing and propagating waves. Figure 2 shows the phase cycle of the propagating-wave component of the first CEOF mode, which explains 59% of the total variance. One sees not only the predominant wavenumber-2 pattern but also the eastward propagation of the SST anomaly in Figure 2. A warm anomaly is initially seen over the central South Pacific, with cold anomalies to the west and east of it. In the following phases, the warm anomaly drifts eastward along with the cold anomalies. At the end of the sequence, part of the warm anomaly passes through Drake Passage.

The Hovmoeller diagrams of first-level temperature and salinity anomalies (Fig. 1) are illustrative for the other ocean levels down to 1000 m except that more coherent and intense anomalies are present over the eastern Pacific and Atlantic sectors than over the Indian and the western Pacific sectors in the interior ocean. The anomalies of the eighth-level (mid-depth: 310 m) ocean temperature and salinity (hereafter referred to as T310 and S310, respectively) are shown in Figure 1 to demonstrate this. The same dominant oscillation period and phase speed are found at these levels. Interestingly, the speed of eastward propagation of temperature and salinity anomalies appears to be independent of depth. As we know, the zonal velocity decreases with depth. In our model, the mean zonal velocity at 56° S is 0.097 m $s^{-1}$ in the upper 100 m, and 0.085 m $s^{-1}$ at 310 m depth. This suggests that, below the surface, advection of the ACC does not play as significant a role in the eastward movement of the anomalies. This seems to support the notion proposed by Bonekamp and others (1999) that the circumpolar character of the marginal stratification in the Southern Ocean allows convection along the trajectory of the surface anomalies, which are advected with the surface ACC. In this way the anomalies can be maintained in time against the turbulent dissipation in the top and intermediate layers. The stronger temperature and salinity anomalies over the eastern Pacific and Atlantic sectors in the interior ocean imply stronger anomalous oceanic convections there.

The eastward propagations of ocean temperature and salinity anomalies in the interior ocean are also found in the model studies of Bonekamp and others (1999) and Cai and others (1999). However, the predominant wavenumber in their models is 3 whereas in our model it is 2. One significant difference between our ocean model and theirs is the higher horizontal and vertical resolutions in our model, allowing us to reasonably simulate the local strength of the ACC which consists of many eddies and narrow jet streams. The coarse-resolution models tend to underestimate the strength of the ACC, although they obtained reasonable Drake Passage transport due to the too wide Drake Passage. Assuming the oceanic part of the ACW is strongly governed by advection

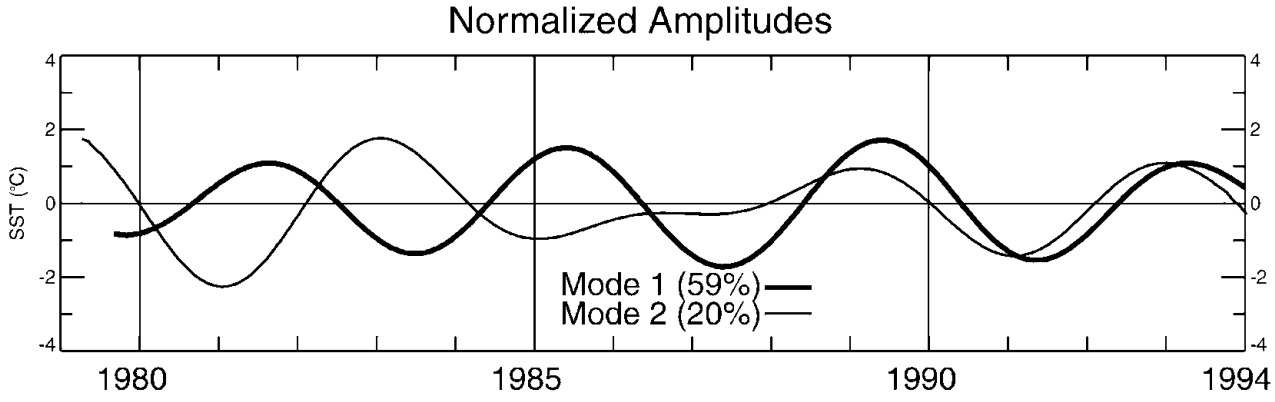


*Fig. 3. Temporal normalized amplitude of the pattern shown in Figure 2. The temporal normalized amplitude for the second mode of the propagating wave of CEOF analysis on the first-level (mid-depth: 12.5 m) ocean temperature is also shown.*


https://doi.org/10.3189/172756401781818644 Published online by Cambridge University Press

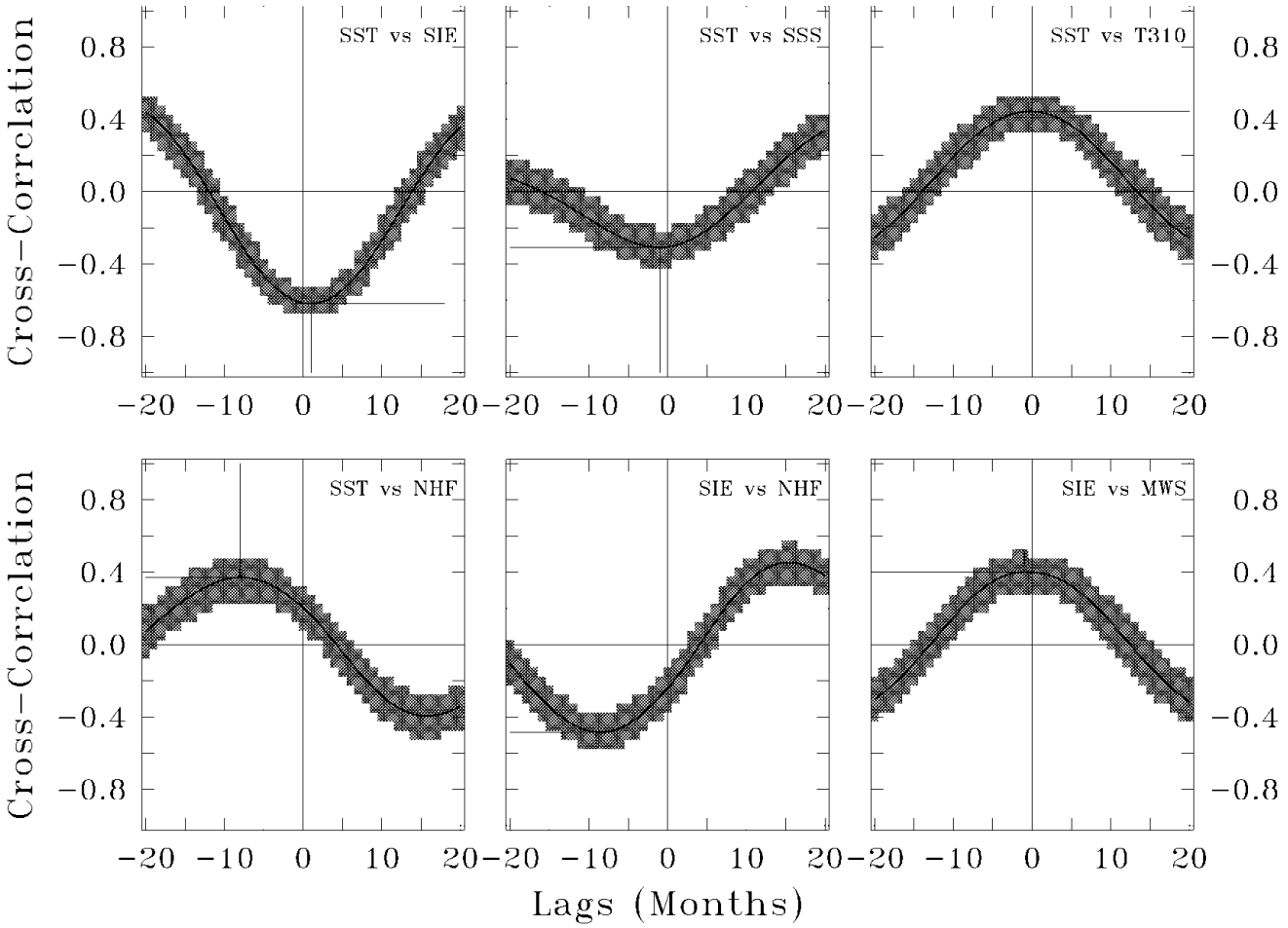


*Fig. 4. Lagged cross-correlations of the filtered monthly anomalies of the indicated variables, averaged along 56° S. Ninety-five per cent confidence intervals are indicated by gray shading (computed according to Fischer's Z-transform). Positive lags indicate the first variable leading the second, and vice versa for the negative lags.*

as claimed by Christoph and others (1998) and Weisse and others (1999), the strength of the ACC would largely determine the time-scale of the oceanic component of the ACW. This may account for the slower phase speed of the oceanic ACW in the model of Bonekamp and others (1999) than in ours, since their simulated average ACC strength is about one-half of ours even though the two models are forced by the same ERA atmospheric forcing.

## 4. PHASE RELATIONSHIP

In this section, the phase relationship among the various variables discussed in section 3 is examined to understand the dynamics of the ACW. Note that the cold (warm) ocean temperature anomalies, northward (southward) SIE anomalies and saltier (fresher) than normal ocean salinity anomalies are in phase (Fig. 1). This phase relationship is confirmed by the almost zero-lag cross-correlations between SST and SIE anomalies, and between SST and SSS anomalies (Fig. 4). The zero-lag cross-correlation between SST and T310 anomalies indicates that the temperature anomalies at the two depths are in phase. The lagged cross-correlations of NHF anomalies vs SST and SIE anomalies show warm (cold) SST and southward (northward) SIE anomalies trailing more (less) than normal downward NHF by about 10 months (or ~90° out of phase). The lagged cross-correlation of MWS vs SIE indicates that northward (southward) MWS anomalies and northward (southward) SIE anomalies are in phase.

This phase relation supports the schematic view of the ACW proposed by White and Peterson (1996, fig. 3) if one overlays less (more) than normal NHF on their high (low) SLP anomalies. (We did not analyze the ERA SLP anomaly because we did not use ERA SLP to force the model.) It can be summarized as follows: less (more) than normal NHF, coinciding with high (low) SLP anomalies, induces northward (southward) MWS anomalies 90° downstream as required by the geostrophic balance; the anomalous advection of cold (warm) air associated with the anomalous northward (southward) MWS cools (heats) the ocean surface, resulting in a cold (warm) SST anomaly; at the same time, the northward (southward) MWS anomaly advects more (less) sea ice northward, and the cooler (warmer) air and ocean allows more (less) sea-ice growth, inducing northward (southward) SIE anomalies; the surface anomalies are advected with the ACC, and the anomalous oceanic convection along the path transports the ACW surface signal downwards and sustains the anomalies against the turbulent dissipation in the top and intermediate layers, especially over the eastern South Pacific and South Atlantic Oceans.

## 5. CONCLUSIONS

This study demonstrates that a one-way atmosphere-to-ocean–ice coupling is sufficient to generate the ACW signature in ocean and sea ice, providing the ACW signature is present in the atmosphere. We cannot determine whether



https://doi.org/10.3189/172756401781818644 Published online by Cambridge University Press

the presence of the ACW in the atmosphere depends on positive feedback from the ocean and sea ice since our model does not interact with the atmosphere. We also do not know whether the existence of the ACW in ERA depends on feedback from the ocean since the SST, used to drive the ECMWF model, is mainly derived from the observational dataset of Reynolds and Smith (1994), which contains the ACW signature (White and Peterson, 1996). However, a recent analysis by S. G. Warren and J. L. Annis (personal communication, 2000) of 100 years from a coupled climate simulation having the same atmospheric resolution as in Christoph and others (1998) but higher oceanic resolution does show the ACW with wavenumber-2 anomalies propagating in both the atmosphere and ocean. This suggests that oceanic feedback to the atmosphere is essential for the correct phase propagation in the atmospheric component of the ACW. Ongoing analysis of this simulation from the Parallel Climate Model of Washington and others (2000) is being pursued by Warren and Annis.

## ACKNOWLEDGEMENTS

We offer sincere thanks to W. Maslowski and R. Tokmakian at the Naval Postgraduate School, Monterey, for their effort in joining the almost-global model to the Arctic model, and kudos especially to J. L. Annis at the Scripps Institution of Oceanography, University of California, San Diego, for performing the CEOF analysis. We gratefully acknowledge support by the DOE CHAMMP and Climate Change Prediction programs and the U.S. National Science Foundation ARCSS and OPP (grant OPP-9980607) programs. Model simulations were performed mainly on Climate Simulation Laboratory computers at the U.S. National Center for Atmospheric Research. The sea-ice concentration derived from the satellite passive-microwave observations was provided by the Earth Observing System Distributed Active Archive Centre at the U.S. National Snow and Ice Data Center.

## REFERENCES

Bonekamp, H., A. Sterl and G. J. Komen. 1999. Interannual variability in the Southern Ocean from an ocean model forced by European Center for Medium-Range Weather Forecasts reanalysis fluxes. *J. Geophys. Res.*, **104**(C6), 13,317–13,331.

Cai, W., P. G. Baines and H. B. Gordon. 1999. Southern mid- to high-latitude variability, a zonal wavenumber-3 pattern, and the Antarctic Circumpolar Wave in the CSIRO coupled model. *J. Climate*, **12**(10), 3087–3104.

Christoph, M., T. P. Barnett and E. Roeckner. 1998. The Antarctic Circumpolar Wave in a coupled ocean–atmosphere GCM. *J. Climate*, **11**(7), 1659–1672.

Comiso, J. C., D. J. Cavalieri, C. L. Parkinson and P. Gloersen. 1997. Passive microwave algorithms for sea ice concentrations: a comparison of two techniques. *Remote Sensing Environ.*, **60**(3), 357–384.

Gloersen, P., W. J. Campbell, D. J. Cavalieri, J. C. Comiso, C. L. Parkinson and H. J. Zwally. 1992. *Arctic and Antarctic sea ice, 1978–1987: satellite passive-microwave observations and analysis*. Washington, DC, National Aeronautics and Space Administration. (NASA SP-511.)

Hunke, E. C. and J. K. Dukowicz. 1997. An elastic–viscous–plastic model for sea ice dynamics. *J. Phys. Oceanogr.*, **27**(9), 1849–1867.

Hunke, E. C. and Y. Zhang. 1999. A comparison of sea ice dynamics models at high resolution. *Mon. Weather Rev.*, **127**(3), 396–408.

Jacobs, G. A. and J. L. Mitchell. 1996. Ocean circulation variations associated with the Antarctic Circumpolar Wave. *Geophys. Res. Lett.*, **23**(21), 2947–2950.

Killworth, P. D., D. Stainforth, D. J. Webb and S. M. Paterson. 1991. The development of a free-surface Bryan–Cox–Semtner ocean model. *J. Phys. Oceanogr.*, **21**(9), 1333–1348.

Large, W. G. and S. Pond. 1982. Sensible and latent heat flux measurements over the ocean. *J. Phys. Oceanogr.*, **12**(5), 464–482.

Levitus, S. 1982. *Climatological atlas of the world ocean*. Rockville, MD, U.S. Department of Commerce. National Oceanic and Atmospheric Administration. (NOAA Professional Paper 13.)

Maslowski, W. 1997. Advanced modeling of the Arctic Ocean and sea ice in support of global climate studies. *In Workshop on Polar Processes in Global Climate, 1997, Cancun, Mexico. Proceedings*. Boston, MA, American Meteorological Society, 93–96.

Parkinson, C. L. and W. M. Washington. 1979. A large-scale numerical model of sea ice. *J. Geophys. Res.*, **84**(C1), 311–337.

Parsons, A. R. 1995. On the Barents Sea polar front in summer and interpretations of the associated regional oceanography using an Arctic Ocean general circulation model. (Ph.D. thesis, Naval Postgraduate School, Monterey, CA.)

Peterson, R. G. and W. B. White. 1998. Slow oceanic teleconnections linking the Antarctic circumpolar wave with the tropical El Niño–Southern Oscillation. *J. Geophys. Res.*, **103**(C11), 24,573–24,583.

Preisendorfer, R. W. 1988. *Principal component analysis in meteorology and oceanography*. Amsterdam, Elsevier Science Publishers.

Qiu, B. and F.-F. Jin. 1997. Antarctic circumpolar waves: an indication of ocean–atmosphere coupling in the extratropics. *Geophys. Res. Lett.*, **24**(21), 2585–2588.

Reynolds, R. W. and T. M. Smith. 1994. Improved global sea surface temperature analyses using optimum interpolation. *J. Climate*, **7**(6), 929–948.

Semtner, A. J., Jr. 1976. A model for the thermodynamic growth of sea ice in numerical investigations of climate. *J. Phys. Oceanogr.*, **6**(5), 379–389.

Semtner, A. J., Jr. and R. M. Chervin. 1992. Ocean general circulation from a global eddy-resolving model. *J. Geophys. Res.*, **97**(C4), 5493–5550.

Washington, W. M. *and 10 others*. 2000. Parallel Climate Model (PCM) control and transient simulations. *Climate Dyn.*, **16**(10–11), 755–774.

Weisse, R., U. Mikolajewicz, A. Sterl and S. S. Drijfhout. 1999. Stochastically forced variability in the Antarctic Circumpolar Current. *J. Geophys. Res.*, **104**(C5), 11,049–11,064.

White, W. B. and R.G. Peterson. 1996. An Antarctic circumpolar wave in surface pressure, wind, temperature and sea-ice extent. *Nature*, **380**(6576), 699–702.

Zhang, Y., W. Maslowski and A. J. Semtner. 1999. Impact of mesoscale ocean currents on sea ice in high resolution Arctic ice and ocean simulations. *J. Geophys. Res.*, **104**(C8), 18,409–18,429.